Variable Bias Current Control and Adaptive Parameter Estimation in Active Magnetic Bearings

Satoshi Ueno*
Ritsumeikan University
Kusatsu, Shiga, Japan

M. Necip Sahinkaya
University of Bath
Bath, UK

Abstract

Reducing the energy consumption of active magnetic bearings is important for some applications to reduce operating cost, expand the operating period, and avoid heat generation. The power loss of magnetic bearings consists of ohmic, electronic circuit, windage, eddy current, and hysteresis losses. With the exception of windage, these losses are functions of the coil currents, therefore, minimization of these has a significant effect on the overall energy efficiency of a magnetic bearing. In this paper, a variable bias current scheme is introduced to minimize the energy consumption without altering the dynamic performance. Since the current stiffness and negative stiffness of the magnetic bearing are functions of the bias current, it is possible to achieve invariant dynamics for various bias current settings. The optimum bias current is calculated from the demand bearing force and instantaneous rotor displacement, but errors in model parameters may result in changes in system dynamics. Therefore, correct parameter values are required for invariant dynamics. In this paper, estimation methods for various parameter errors are introduced and verified experimentally. The proposed variable bias current controller and parameter estimation methods yield significant energy savings, are simple to implement and applicable to a wide range of magnetic bearing systems.

1 Introduction

The areas of application of magnetic bearings are steadily expanding because of the significant advantages they offer compared with conventional bearings [1]. They provide contact-free and oil-free support of rotating machinery without the friction losses in oil film bearings. They can operate in hostile environments, at very high temperatures, and at high speeds. They are also an ideal choice in applications where contamination is an issue such as turbo-molecular pumps and artificial hearts. The power loss in magnetic bearings is lower than for fluid film bearings, but there is potential for further significant reduction [2, 3]. Low power consumption is important in several application areas, such as high-speed energy storage flywheel systems, transport applications where the energy is provided by a battery, and micro/nano applications.

A constant bias current linearization is often used in active magnetic bearings to stabilize rotor dynamics. This approach provides a simple mathematical model, and uncomplicated controller design and implementation. However, a fixed bias current is inefficient under small load conditions. A variable bias current control method proposed in [4, 5, 6] showed that an optimum value can be calculated analytically for a desired bearing stiffness, static load and orbit size of the rotor. In order to realize the optimum bias current, linear and nonlinear variable bias current controllers were introduced. A linear controller is simple to implement and allows easy gain tuning, but the control performance becomes poor in the case of small bias current and large displacement. The nonlinear controller can overcome these problems, but it requires more precise bearing parameters.

In this paper, the bearing force incorporating the effect of parameter errors are derived analytically and variable bias current controllers are introduced. Then the affects of parameter errors on the system dynamics when the bias current changes are discussed, and the estimation methods of

*sueno@se.ritsumei.ac.jp, 1-1-1 Nojihigashi, Kusatsu, Shiga 525-8511, Japan

the parameter errors are introduced. The proposed estimation methods and the variable bias current controllers are assessed through experiments.

2 Bearing Force with Parameter Errors

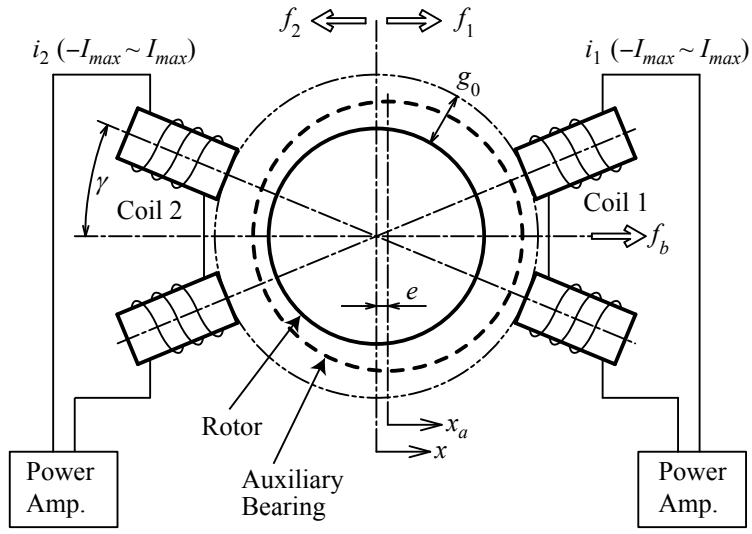

Figure 1: Schematic View of AMB System

2.1 Bearing Force and Normalization

Figure 1 shows a schematic view of an AMB system. Two opposing poles generate a bidirectional force along the horizontal axis. The displacement from the center of two electromagnets is defined as x. Usually an auxiliary bearing is used for avoiding contact between the rotor and stator. The sensors are usually aligned with respect to the auxiliary bearing center. However, it may be difficult to align the auxiliary bearing center with the magnetic center [7]. Therefore the displacement from the auxiliary bearing center is defined as x_a. The difference between x and x_a is termed the magnetic center misalignment, and denoted as $e(= x_a - x)$. The physical air gap is defined as g_0. The poles are excited by the coil currents i_1 and i_2 applied by 4-quadrant power amplifiers. In the differential current control mode, the control current is added and subtracted from the bias current to generate driving currents for both coils as follows:

$$i_1 = i_b + i_c \quad \text{and} \quad i_2 = i_b - i_c \tag{1}$$

It is important to note that the control current i_c includes both static and dynamic components. The range of the coil currents is from $-I_{max}$ to I_{max}. In the experimental magnetic bearing system, 2-quadrant amplifiers are used for implementation. However, since the magnetic force is proportional to the square of the coil current, the negative coil current can be implemented by using the absolute value.

The bearing force can be written as follows:

$$f_b = \frac{\hat{l}_0 + l_e}{2(\hat{x}_0 + x_e - x_a + e)^2} {i_1}^2 - \frac{\hat{l}_0 + l_e}{2(\hat{x}_0 + x_e + x_a - e)^2} {i_2}^2 \tag{2}$$

where $\hat{x}_0$ is a nominal equivalent air gap and x_e is the error between the nominal and real value. The nominal effective self-inductance at unit air gap, $\hat{l}_0$, is defined as

$$\hat{l}_0 = \frac{\mu_0 A_p N_a^2}{2} \cos\gamma \tag{3}$$

where μ_0 is the permeability of free space, A_p is the pole area, N_a the number of windings and γ is the half angle between double pole faces. The error between $\hat{l}_0$ and the real value is defined as l_e. Generally, the bearing force is influenced by magnetic saturation, hysteresis, and eddy current. However, these effects are small in the test rig and are neglected in this paper.

In order to generalize the analysis, normalized variables are used. The normalized variables are denoted by capitalized symbols and the normalization constants are shown in Table 1, where F_{max} is the maximum force at the magnetic center. The normalized magnetic force can be written as

$$F_b = \frac{1 + L_e}{(1 + X_e - X_a + E)^2} (I_b + I_c)^2 - \frac{1 + L_e}{(1 + X_e + X_a - E)^2} (I_b - I_c)^2 \tag{4}$$

where

$$X_e = \frac{x_e}{\hat{x}_0}, \quad L_e = \frac{l_e}{\hat{l}_0} \quad \text{and} \quad X_a = X + E = \frac{x}{\hat{x}_0} + \frac{e}{\hat{x}_0} \tag{5}$$

Variable	Unit	Constant
Displacement	m	$\hat{x}_0$
Force	N	$F_{max} = \hat{l}_0 I_{max}^2 / (2\hat{x}_0^2)$
Mechanical Stiffness	N/m	$F_{max}/\hat{x}_0$
Current Stiffness	N/A	F_{max}/I_{max}
Current	A	I_{max}
Power	W	RI_{max}^2

Table 1: List of Normalization Constants

2.2 Linearization

In the presence of a nonzero static force F_0, the bias currents on the opposing poles provide a constant static force to counteract F_0. Hence coil currents are expressed as:

$$I_1 = I_b + I_{c0} + I_{cd} \quad \text{and} \quad I_2 = I_b - I_{c0} - I_{cd} \tag{6}$$

where I_{c0} produces the static force and I_{cd} is the dynamic component of the control current. Substituting Eq. (6) into (4), and calculating a Taylor expansion for small X and I_{cd} in the neighborhood of $X_a = 0$, $E = 0$ and $I_{cd} = 0$, the approximate linearized magnetic force can be obtained as follows:

$$F_b \approx \frac{4(1 + L_e)}{(1 + X_e)^2} I_b I_{c0} + \frac{4(1 + L_e)}{(1 + X_e)^2} I_b I_{cd} + \frac{4(1 + L_e)}{(1 + X_e)^3} (I_b^2 + I_{c0}^2)(X_a - E) \tag{7}$$

3 Variable Bias Current Controller

3.1 Control Force

Because of their inherent negative stiffness properties, magnetic bearings are unstable and require position feedback for stability. The control force demand, F_c, is generated by using a PID controller:

$$F_c = F_{cd} + F_{c0} = -K_p X_a - K_d \frac{d}{dt} X_a - \left(\hat{F}_0 + K_i \int X_a dt \right) \tag{8}$$

where F_{cd} and F_{c0} are the dynamic and static components of the control force demand, $\hat{F}_0$ is the nominal value of the static load, K_p, K_d and K_i are the normalized proportional, derivative and integral gains, respectively. The first two terms of the right side of Eq. (8) correspond to the dynamic component F_{cd}, and the others the static component F_{c0}.

3.2 Nonlinear Controller

Since the parameter errors are unknown, the coil currents for the nonlinear controller can be obtained by solving the nonlinear bearing force equation with $L_e = X_e = E = 0$ as follows:

$$I_c = \begin{cases} \text{no solution} & X_a = I_b = 0,\ F_c \neq 0 \quad (a) \\ \text{any} & X_a = I_b = F_c = 0 \quad (b) \\ \dfrac{1}{4I_b} F_c & X_a = 0,\ I_b \neq 0 \quad (c) \\ -\dfrac{1+{X_a}^2}{2X_a} I_b + \dfrac{1-{X_a}^2}{2X_a} \sqrt{I_b^2 + X_a F_c} & X_a \neq 0 \quad (d) \end{cases} \tag{9}$$

The conditions required for a solution (i.e. positive value in the square root) are:

$$\begin{aligned} F_c &\geq -\frac{1}{X_a} I_b^2 \qquad X_a > 0 \\ F_c &\leq -\frac{1}{X_a} I_b^2 \qquad X_a < 0 \end{aligned} \tag{10}$$

Taking the partial derivative of Eq. (4) with respect to I_c and equating it to zero for the case of $L_e = X_e = E = 0$ gives the extreme value of the control current:

$$I_{c,extreme} = -\frac{1+X_a^2}{2X_a} I_b \tag{11}$$

Then the bearing force at the extreme point becomes

$$F_{b,extreme} = -\frac{1}{X_a} I_b^2 \tag{12}$$

Thus Eq. (10) accords with the extreme bearing force. Moreover, the first term of Eq. (9)(d) corresponds to the extreme control current. Therefore, the control current is automatically restricted within the attainable range by using the real part of Eq. (9). Figure 2 shows the block diagram of the nonlinear variable bias current controller.

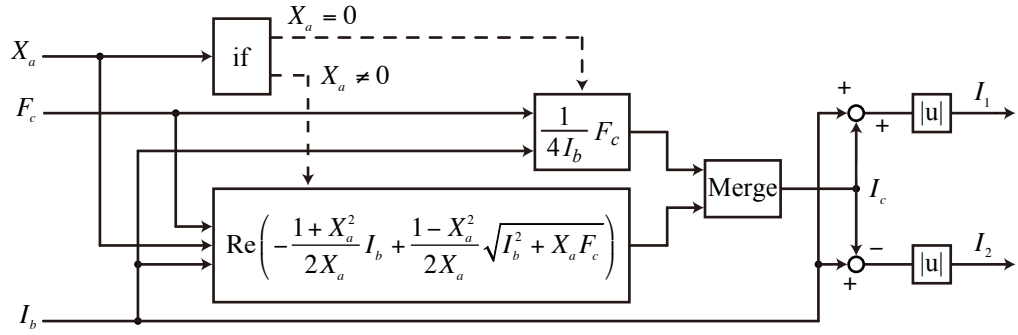

Figure 2: Block Diagram of Nonlinear Variable Bias Current Controller

3.3 Linear Controller

The coil currents are expressed as Eq. (6); I_{c0} can be calculated from Eq. (7) with $F_b = F_{c0}$, $I_{c0} = 0$, $X_a = 0$ and $L_e = X_e = E = 0$, then we have

$$I_{c0} = \frac{F_{c0}}{4I_b} \tag{13}$$

The dynamic components of the control currents can be obtained by solving for the linearized bearing force as follows:

$$I_{cd} = \begin{cases} \text{no solution} & I_b = 0 \\ \dfrac{1}{4I_b} F_{cd} - \dfrac{1}{4I_b}\left(4I_b^2 + \dfrac{F_{c0}^2}{4I_b^2}\right) X_a & I_b \neq 0 \end{cases} \tag{14}$$

For the case of a large rotor displacement and a large control current, the electromagnet will produce a bearing force in opposite directions due to their non-linearity, hence the control current should be limited by the extreme value of the bearing force. Then the current limit can be expressed as follows:

$$\begin{cases} I_c > -\dfrac{1+X_a^2}{2|X_a|} I_b & X_a \geq 0 \\ I_c < -\dfrac{1+X_a^2}{2|X_a|} I_b & X_a < 0 \end{cases} \tag{15}$$

Figure 3 shows the block diagram of the linear variable bias current controller.

3.4 Optimum Bias Current

The losses of an active magnetic bearing are ideally coincident with the copper loss in the coils. The normalized copper loss can be calculated as:

$$P_{cl} = \frac{p_{cl}}{RI_{max}^2} = (I_b + I_c)^2 + (I_b - I_c)^2 = 2(I_b^2 + I_c^2) \tag{16}$$

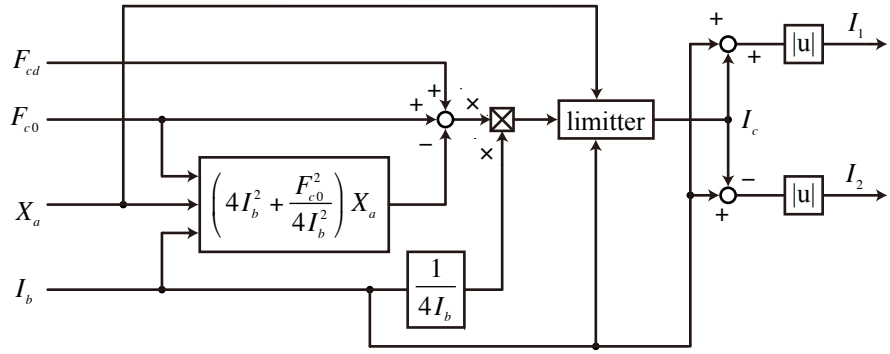

Figure 3: Block Diagram of Linear Variable Bias Current Controller

Substituting Eq. (9) into (16), we have

$$P_{cl}=\begin{cases} 2I_b^2+\dfrac{1}{8I_b^2}F_c^2 & X_a=0 \\ \left(X_a^2+\dfrac{1}{X_a^2}+2\right)I_b^2+\dfrac{1}{2}\left(X_a^2+\dfrac{1}{X_a^2}-2\right)X_aF_c+\left(X_a^2-\dfrac{1}{X_a^2}\right)I_b\sqrt{I_b^2+X_aF_c} & X_a\neq 0 \end{cases} \tag{17}$$

The optimum bias current can be obtained by minimizing the copper loss. Differentiating P_{cl} with respect to I_b and equating it to zero gives

$$I_{b,opt}=\begin{cases} \dfrac{1-X_a}{2}\sqrt{F_c} & F_c\geq 0 \\ \dfrac{1+X_a}{2}\sqrt{-F_c} & F_c<0 \end{cases} \tag{18}$$

4 Parameter Errors

4.1 Effects of Errors

First, the static balance is considered. In this case, the rotor displacement converges to zero with the help of the integral action. Substituting Eq. (9) with $X_a=0$ into Eq. (4), the bearing force becomes

$$F_b=-\frac{4(1+L_e)(1+X_e)E}{(1+X_e)^2-E^2}I_b^2-\frac{(1+L_e)(1+X_e)E}{4\{(1+X_e)^2-E^2\}}\frac{F_c^2}{I_b^2}+\frac{(1+L_e)\{(1+X_e)^2+E^2\}}{2\{(1+X_e)^2-E^2\}}F_c \tag{19}$$

This can be approximated by linearization to give

$$F_b\approx\frac{1+L_e}{(1+X_e)^2}F_{c0}-\frac{(1+L_e)}{(1+X_e)^3}\left(4I_b^2-\frac{F_{c0}^2}{4I_b^2}\right)E \tag{20}$$

These results show that the bearing force is affected by changes in the bias current when the auxiliary center is not coincident with the magnetic center.

Next, the dynamic force is considered. Since the magnetic center can be obtained from the static balance, for simplicity the center positional error is neglected. Substituting Eq. (9) into Eq. (4) with $E = 0$ gives

$$F_b = 2X_e(1+L_e)\frac{(X_a^2+1)(X_a^2-1-X_e)}{X_a\{(1+X_e)^2-X_a^2\}}I_b^2 + 2X_e(1+L_e)\frac{(X_a^2-1)(X_a^2-1-X_e)}{X_a\{(1+X_e)^2-X_a^2\}}I_b\sqrt{I_b^2+X_aF_c} + (1+L_e)(1+X_e)\left\{\frac{1-X_a^2}{(1+X_e)^2-X_a^2}\right\}^2 F_c \tag{21}$$

This can be linearized to give

$$F_b \approx \frac{1+L_e}{(1+X_e)^2}(F_{c0}+F_{cd}) - \frac{1+L_e}{(1+X_e)^3}\left(4I_b^2+\frac{F_{c0}^2}{4I_b^2}\right)X_eX_a \tag{22}$$

These results show that the bearing force is not affected by the bias current variation only when X_e is zero.

Finally, L_e is considered. Substituting Eq. (9) into Eq. (4) with $E = 0$ and $X_e = 0$, the bearing force becomes

$$F_b = (1+L_e)F_c \tag{23}$$

Thus the bearing force is not affected by the bias current variation.

4.2 Estimation of Parameter Errors

First, consider the center positional error: If this is non-zero, the rotor will move by changing the bias current due to a change of the bearing force. Hence it is possible to estimate the center position by forced fluctuation of the bias current. Partial differential of Eq. (20) with respect to I_b gives

$$\frac{\partial F_b}{\partial I_b} = -\frac{1+L_e}{(1+X_e)^3}\left(8I_b+\frac{F_{c0}^2}{2I_b^3}\right)E \tag{24}$$

Since the range of I_b is from 0 to 1, if E is positive, the bearing force will increase by decreasing the bias current ($\dot{I}_b < 0$), then the rotor velocity will be positive ($\dot{X} > 0$). If $E > 0$ and $\dot{I}_b > 0$, the bearing force will decrease and the rotor velocity will be negative ($\dot{X} < 0$). Hence it is possible to know the sign of E from $\dot{X}/\dot{I}_b$, then E can be estimated by

$$E = -\int K\frac{\dot{X}}{\dot{I}_b}dt \tag{25}$$

The block diagram of the center position estimator is shown in Fig. 4. For simplicity a triangular waveform, for which $\dot{I}_b$ is constant, is used for the bias current.

The equivalent airgap X_0 can be corrected by examining the rotor dynamics. The disturbance (test) signal is injected into the control force as shown in Fig. 5. The transfer function from F_d to X is

$$G(s) = \frac{X(s)}{F_d(s)} = \frac{1}{\dfrac{(1+X_e)^2}{1+L_e}Ms^2 + K_ds + K_p + \left(4I_b^2+\dfrac{F_{c0}^2}{4I_b^2}\right)\dfrac{X_e}{1+X_e}} \tag{26}$$

This result shows that the error in the airgap affects the bearing stiffness. Hence, the correct airgap can be obtained by investigating the stiffness of the magnetic bearing for various bias currents.

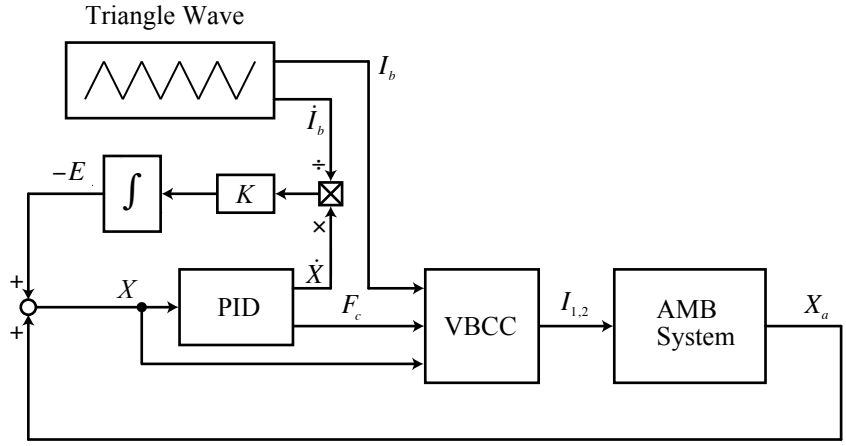

Figure 4: Adaptive Center Position Estimator

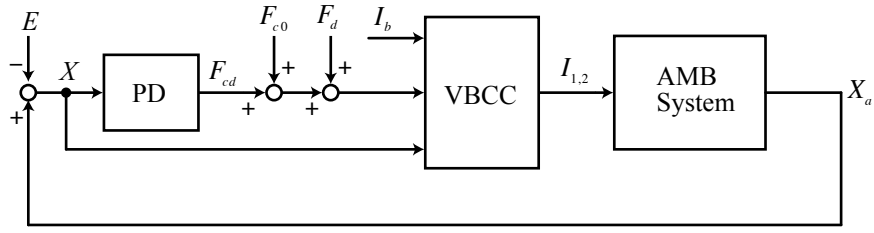

Figure 5: Disturbance Signal

5 Experimental Results

5.1 Test Rig

Experiments were performed using the test rig shown in Fig. 6. The rotor consists of a uniform flexible steel shaft of length 2 m and radius 0.025 m, with four 10 kg disks of radii 0.125 m. The total rotor mass is 100 kg and it is mounted horizontally on two radial magnetic bearings. The coils were placed at an angle of 45° to the vertical, hence the static load at each axis was 347 N. The control current of the magnetic coils was supplied through eight amplifiers. The design parameters of the magnetic bearing are shown in Table 2. Eight eddy current displacement sensors were placed at four planes with a 45° angle to the vertical line. The sensors are calibrated with respect to the auxiliary bearing center.

A dSPACE digital signal processor (DSP) was used to implement the control algorithm. The rotor was assumed to be rigid because the experiments were conducted at 10 Hz, which is well below the first flexural critical speed of 30 Hz. An approximate derivative was used for the PID controller. The transfer function of the PID controller is

$$G_{PID}(s) = k_p + k_d \frac{s}{s/\omega_b + 1} + \frac{k_i}{s} \tag{27}$$

The controller was transformed to a discrete transfer function by the bilinear transformation, and then implemented by the DSP. The control parameters are given in Table 3.

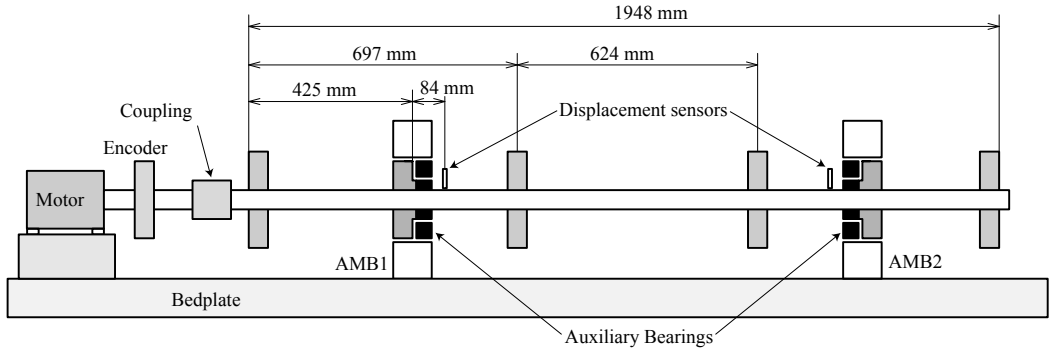

Figure 6: A View of the Experimental Rotor AMB System

Variable	Value	Unit
I_{max}	10	A
l_0	84.5×10^{-6}	Hm
g_0	1.3×10^{-3}	m
R	0.365	Ohm
F_{max}	2,500	N
F_{max}/g_o	1.928×10^6	N/m
F_{max}/I_{max}	250	NA

Table 2: Specifications of the Magnetic Bearing

Variable	Value	Unit
k_p	2×10^6	N/m
k_d	5,000	Ns/m
ω_b	1,500	rad/s
k_i	0.3×10^6	N/m/s
Sampling time	0.25	ms

Table 3: Parameters of the Controller

5.2 Preliminary Test

Figure 7 shows the time responses of the bias current optimization without parameter corrections at 10 Hz rotation. The linear variable bias current controller was used. The upper graph of each axis is the rotor displacement, the second is the bias current, and the third one is the ohmic loss in the coils. The bias current was switched from 5 A to the optimum value at $t = 0$ s. The bias currents were decreased immediately at $t = 0$. The displacement and amplitude of the vibration were affected by the bias current change because of the existence of parameter errors. The ohmic loss was reduced by about 73%.

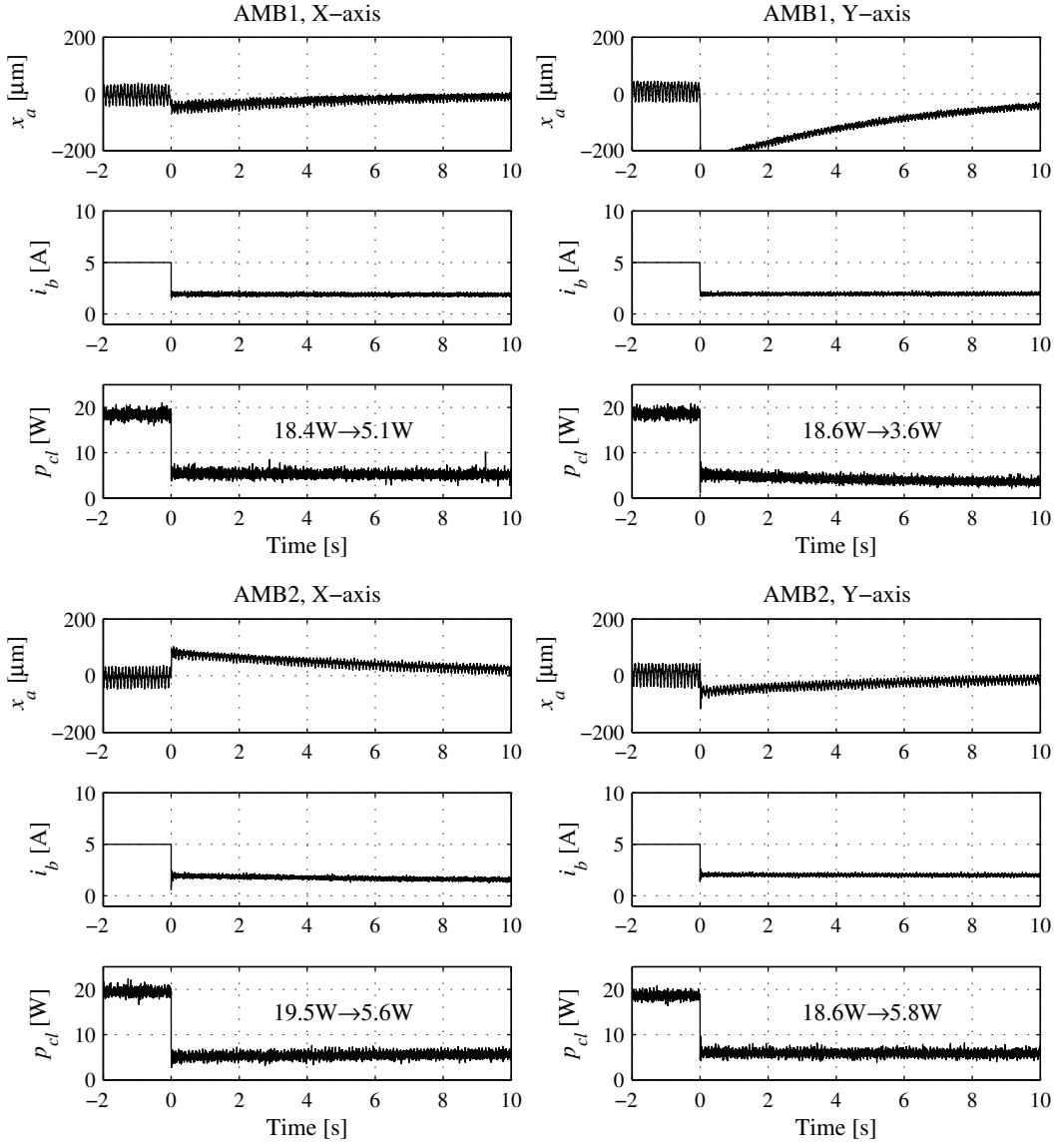

Figure 7: Results of the bais current optimization with nominal parameters

5.3 Parameter Estimation

The experimental results of the adaptive estimation of the magnetic center position are shown in Fig. 8. The initial value of e was set to 0, current $\dot{i}_b$ was ± 6.25 A/s, within a range of i_b from 2.5 to 5 A, and the gain K was set to 10. The parameter estimation was carried out with the linear variable bias current controller.

The top graph of each axis shows the bias current, the second and third are the sensor output and the estimated error, respectively. In every case, the error converges in about 60 s, and the amplitude of vibration due to the bias current variation was suppressed. Both a positive and negative error

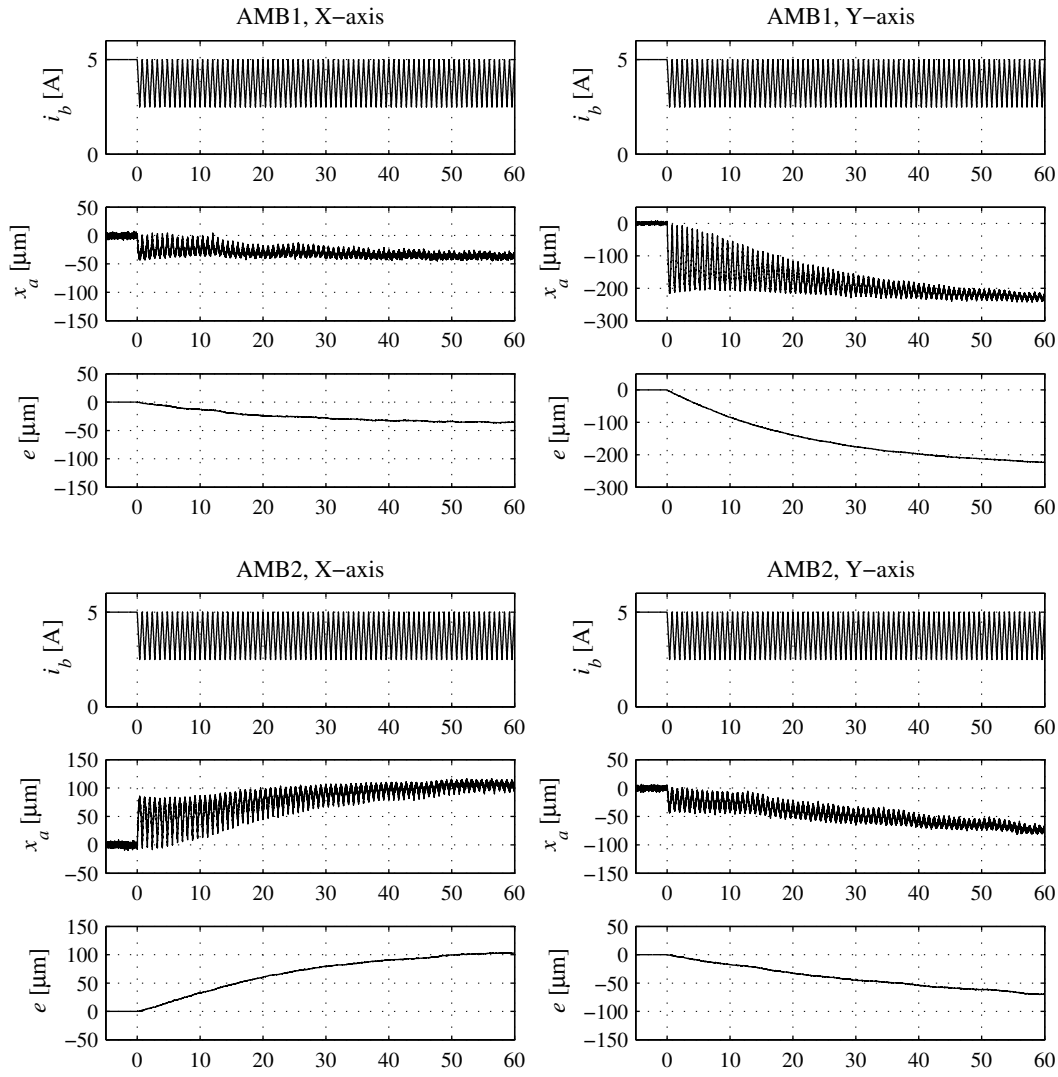

Figure 8: Experimental Results of the Adaptive Estimation of the Magnetic Center Position

can be estimated. Results confirmed that the proposed method is effective for the estimation of the magnetic center position.

The error between the magnetic center and auxiliary center can be approximated by a sinusoidal function of the rotor angular position. The measured results are shown in Fig. 9. These can be obtained easily with the help of the adaptive center position estimator.

Figure 10 shows measured results of the bearing stiffness as a function of the bias current for various values of $\hat{x}_0$, which was changed from 1.1 mm to 1.35 mm at intervals of 0.05 mm. The lines show the theoretical values. These results show that the constant stiffness can be obtained by using the correct x_0 value. The estimated x_0 are shown in the each graph. These values were constant regardless of the angular position of the rotor.

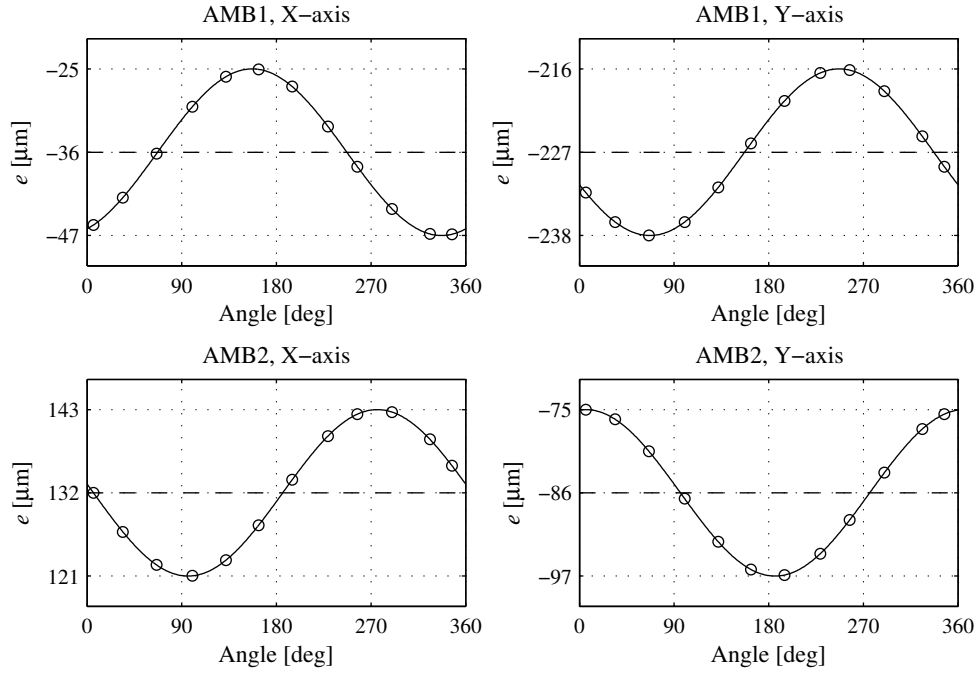

Figure 9: Measured Misalignment Between Magnetic and Auxiliary Bearing Centers

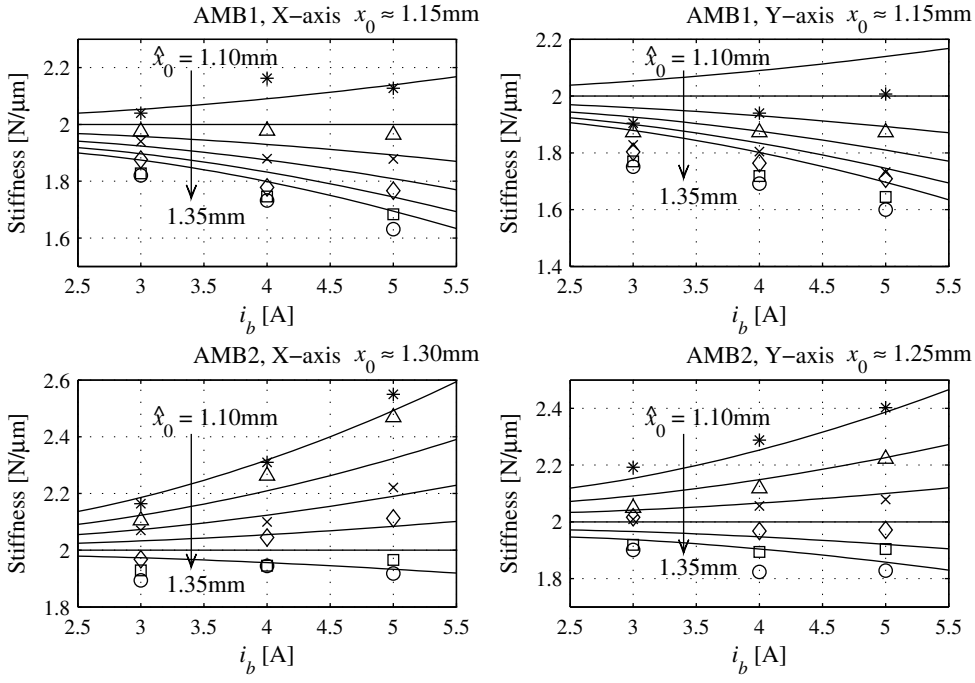

Figure 10: Estimated Bearing Stiffness for Various $\hat{x}_0$ and Bias Current Settings

5.4 Optimization of the Bias Current

The tests of the bias current optimization were carried out with the correct parameters. Figure 11 shows the results of the rotational tests. The upper graph of each axis shows the corrected displacement, while the lower one shows the sensor output. The bias current was switched at $t = 0$ s from 5 A to the optimum value. The effect bias current variations on the rotor response were reduced significantly, and the effectiveness of the parameter correction method was confirmed.

Figure 12 shows the orbits of the rotor with a large sinusoidal disturbance signal of 400 N amplitude at 32 Hz. Figure 12(a) shows the results using the linear controller, while (b) shows the results using the nonlinear controller. The orbit of the nonlinear controller was nearly circular for the case where the optimum bias current was applied. Thus it was demonstrated that the nonlinear controller is capable of operating large bearing forces and displacements are required.

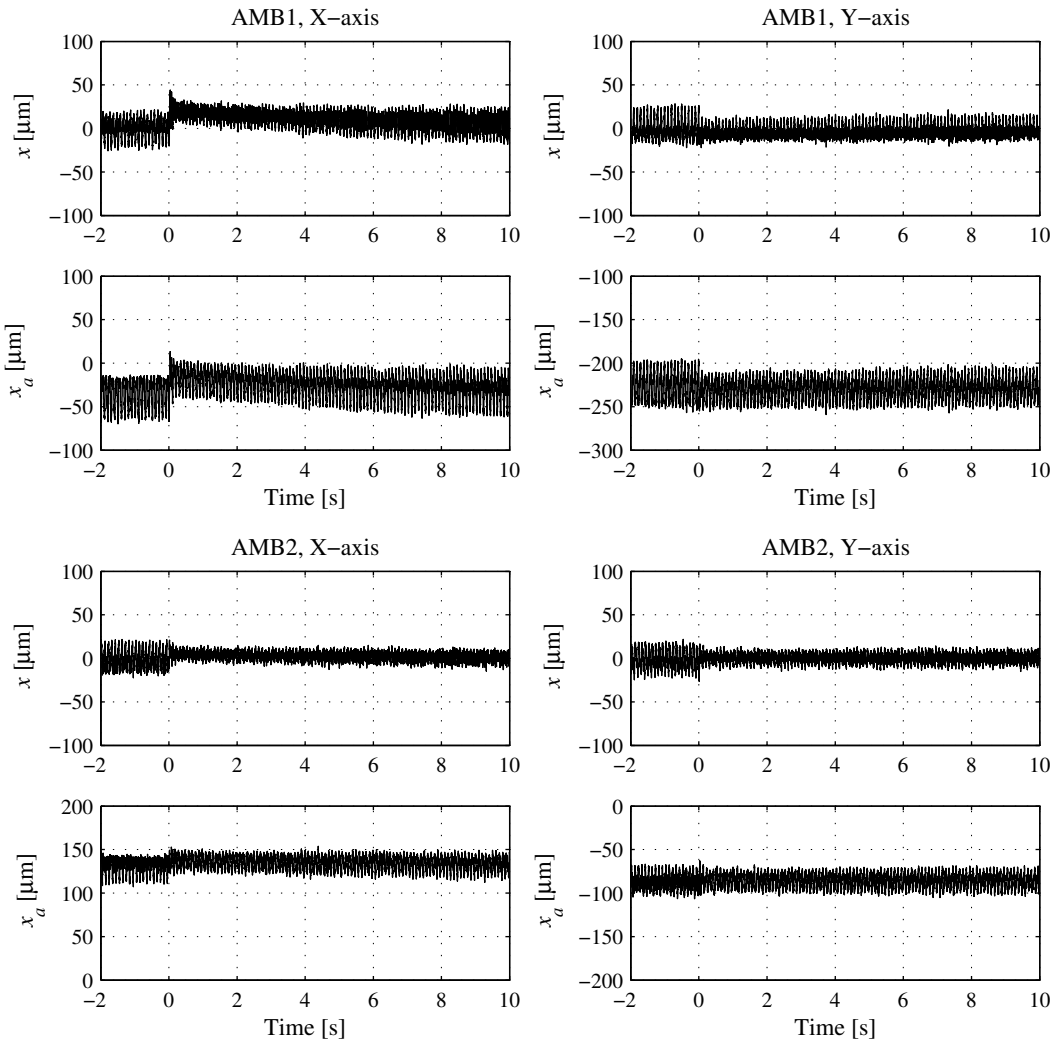

Figure 11: Results of the bias current optimization with correct parameters

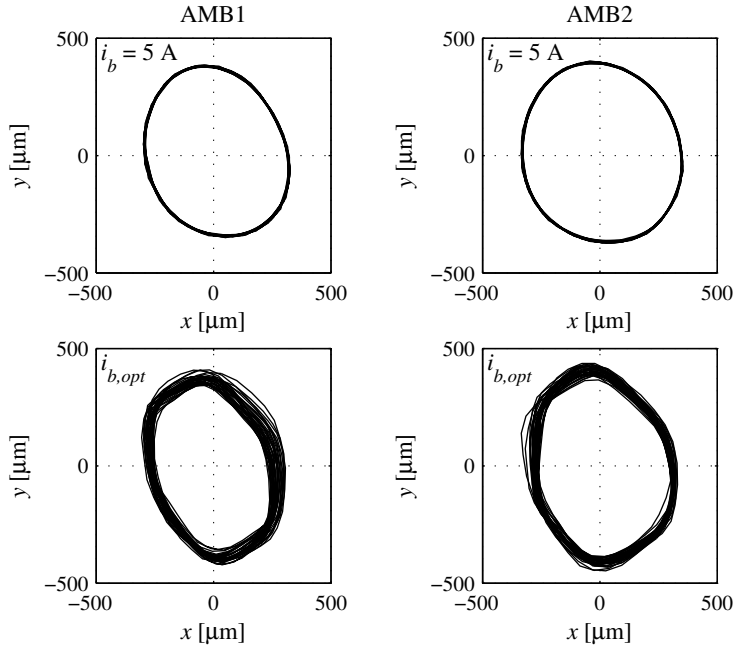

(a) Linear Variable Bias Current Controller

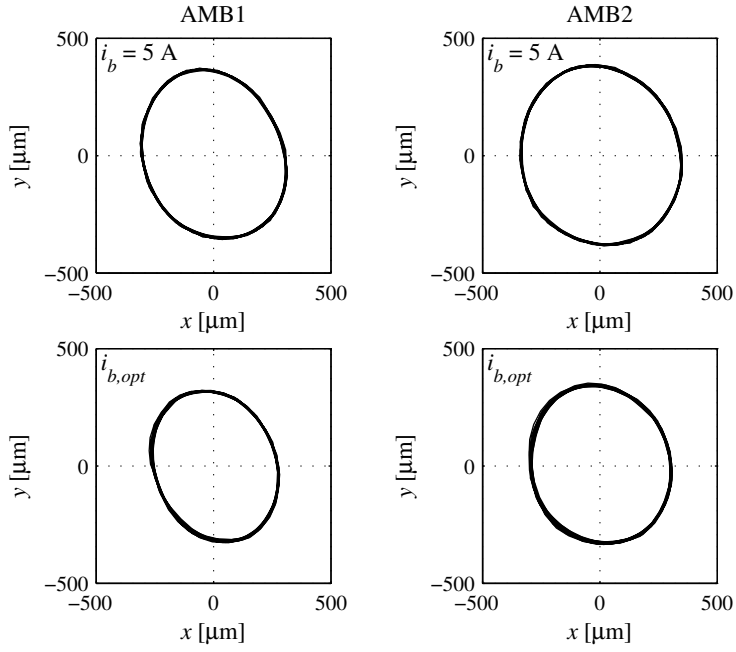

(b) Nonlinear Variable Bias Current Controller

Figure 12: Orbits with Large Disturbance Signal without Rotation

6 Conclusions

The bearing force of the active magnetic bearings with parameter errors was discussed. The nonlinear and linear variable bias current controllers were proposed, and the expressions for optimum bias current values were derived. The effects of the parameter errors were analyzed and correction methods were introduced. Experimental results confirmed that the correct magnetic center position can be obtained by using the adaptive center position estimator. It was shown that the variable bias controller and the optimum bias current achieved 73% energy saving without deterioration of the dynamic performance.

References

[1] Schweitzer, G., 2002. "Active magnetic bearings - chances and limitations". In IFToMM Sixth International Conference on Rotor Dynamics, Vol. 1, Sydney, Australia, pp. 1–14.

[2] Pichot, M. A., and Driga, M. D., 2005. "Loss reduction strategies in design of magnetic bearing actuators for vehicle applications". *IEEE Transactions on Magnetics*, **41**(1), pp. 492–496.

[3] Allaire, P. E., 1999. "Rotor power losses in planar radial magnetic bearings - effects of number of stator poles, air gap thickness, and magnetic flux density". *Journal of Engineering for Gas Turbines and Power-Transactions of the ASME*, **121**(4), pp. 691–696.

[4] Sahinkaya, M. N., Hartavi, A. E., Burrows, C. R., and Tuncay, R. N., 2004. "Bias current optimization and fuzzy controllers for magnetic bearings in turbo molecular pumps". In The Ninth International Symposium on Magnetic Bearings (ISMB9), Lexington, USA.

[5] Sahinkaya, M. N., and Hartavi, A. E., 2007. "Variable bias current in magnetic bearings for energy optimization". *IEEE Transactions on Magnetics*, **43**(3), pp. 1052–1060.

[6] Ueno, S., Sahinkaya, M. N., 2011. "Adaptive bias current control in active magnetic bearings for energy optimization". ASME 2011 International Design Engineering Technical Conferences & Computers and Information in Engineering Conference (IDETC).

[7] Prins, R. J., Kasarda, M. E. F., and Prins, S. C. B., 2007 "A system identification technique using bias current perturbation for determining the effective rotor origin of active magnetic bearings". *Journal of Vibration and Acoustics-Transactions of the ASME*, **129**(3), pp. 317–322.